JOURNAL OF GUIDANCE, CONTROL, AND DYNAMICS
Vol. 32, No. 1, January–February 2009

Engineering Notes

ENGINEERING NOTES are short manuscripts describing new developments or important results of a preliminary nature. These Notes should not exceed 2500 words (where a figure or table counts as 200 words). Following informal review by the Editors, they may be published within a few months of the date of receipt. Style requirements are the same as for regular contributions (see inside back cover).

Inertial Measurements from Flight Data of a Flapping-Wing Ornithopter

Jared A. Grauer* and James E. Hubbard Jr.†
University of Maryland, College Park, Maryland 20742

DOI: 10.2514/1.37495

I. Introduction

ORNITHOPTERS may be classified as aerodynes that generate lifting and thrusting forces from the flapping of wings. The miniaturization of electronics packages from advances in microelectromechanical systems (MEMS) and very-large-scale integration technologies, coupled with the manufacture of lightweight, composite materials, has facilitated the practical realization of small ornithoptic aircraft [1,2]. Although having their own set of drawbacks, flapping-wing designs enjoy numerous advantages over fixed-wing and rotary-wing counterparts at small scales and low Reynolds number flows. For example, fixed-wing aircraft are a natural choice for vehicle designs as their dynamics are well understood. However, these vehicles suffer from a decrease in aerodynamic efficiency as airfoils are scaled to the point where viscous effects become significant [3]. Miniature rotary-wing aircraft are maneuverable and can hover, but have large power requirements and are commonly limited to indoor flight [4]. In contrast, it is envisioned that the nimble flight exhibited by ornithopters can be harnessed to achieve agility and maneuverability on par with birds and insects. Smaller ornithopters can achieve hover, whereas larger ornithopters are robust enough to fly both slowly and quickly in outdoor environments against strong winds. Donning an avian appearance, ornithopters also have a degree of contextual camouflage, which makes them well suited for missions including surveillance, atmospheric data collection, crop surveying, wildlife population monitoring, and airport wildlife control.

A vital component of an aircraft avionics package is the inertial measurement unit (IMU). Typically consisting of magnetometers, gyroscopes, and accelerometers, an IMU provides information on the orientation, rotational velocity, and linear acceleration of the vehicle. These measurements can be fused directly in simple attitude estimation filters [5], or can be incorporated into model-based state observers [6]. This work is an experimental exploration of ornithopter flight dynamics through inertial measurements, which contrasts numerical simulations based on first-principle models [7–9]. The ornithopter test vehicle is introduced, followed by an explanation of the notation and convention used, as well as a description of the configuration-dependant mass distribution of the ornithopter. The avionics hardware developed is then discussed. Flight data are presented and measurements are analyzed in both the time and frequency domains. Ensemble averaging techniques are applied to form a set of representative waveforms and statistics over the duration of a wing stroke. Implications and future work are discussed.

Presented as Paper 224 at the 46th AIAA Aerospace Sciences Meeting and Exhibit, Reno, Nevada, 7–10 January 2008; received 19 March 2008; revision received 25 August 2008; accepted for publication 25 August 2008.

*Graduate Student, Department of Aerospace Engineering. Member AIAA.

†Langley Distinguished Professor, Department of Aerospace Engineering. Associate Fellow AIAA

II. Ornithopter Test Aircraft

A. Overview

The ornithopter used in this study, shown in Fig. 1, is a modified version of the Slow Hawk II series of ornithopter produced by Sean Kinkade.‡ Although both smaller and larger ornithopters are available, this model was selected for its relative ease of flying and available payload. The wing sail is an arrangement of rip–stop polyester segments, fastened together with Dacron tape. Although a flexible membrane, the wing shape is maintained with a primary carbon fiber spar spanning the leading edge, a secondary carbon fiber spar running from the aft section of the ornithopter to the wing tip, and a set of small carbon fiber spars spread along the trailing edge. The fuselage is cut from a 3.2-mm-thick carbon fiber sheet. The aircraft nose has been reinforced with additional plies of carbon fiber to keep the vehicle robust to flight testing.

The ornithopter is flown in the same manner as other remotely controlled vehicles: a pilot launches the ornithopter and uses a 72 MHz transmitter to broadcast joystick commands to an onboard receiver, which in turn directs power from a battery to the actuators. The throttle joystick u_{thr} is used to drive a dc motor and control the flapping frequency, which adjusts the amplitudes of the lift and thrust forces. The longitudinal joystick u_{lon} and lateral joystick u_{lat} control servomotors that pitch and roll the tail relative to the fuselage to impart aerodynamic pitching and coupled rolling/yawing torques on the aircraft center of mass, respectfully.

B. Notation and Sign Convention

Standard aircraft notation [10] was used in defining coordinate frames, state variables, and control deflections. The inertial frame $K_I = \{\mathbf{e}_{xI}, \mathbf{e}_{yI}, \mathbf{e}_{zI}\}$ is placed at an arbitrary point on the surface of the Earth with axes facing north, east, and down. The body frame $K_B = \{\mathbf{e}_{xB}, \mathbf{e}_{yB}, \mathbf{e}_{zB}\}$ is fixed to the aircraft center of mass with axes pointing out the nose, starboard wing, and bottom of the aircraft. The orientation of the body frame with respect to the inertial frame is parameterized by the Euler angles $\boldsymbol{\eta} = [\phi, \theta, \psi]^T$. The aircraft has body-fixed translational velocity $\mathbf{v}^B = [u, v, w]^T$, translational acceleration $\mathbf{a}^B = [a_x, a_y, a_z]^T$, and rotational velocity $\boldsymbol{\omega}^B = [p, q, r]^T$. The offset and alignment of the inertial measurement unit coordinate frame $K_s = \{\mathbf{e}_{xS}, \mathbf{e}_{yS}, \mathbf{e}_{zS}\}$ relative to the body frame are described by the vector $\mathbf{r}_{SB}$ and the rotation matrix $\mathbf{R}^{SB}$, respectfully.

Sign conventions for the control deflections are shown in Fig. 2. The wing angle $\theta_1 \in [-25 \text{ deg}, +25 \text{ deg}]$ is defined as the roll angle of the left wing about the $\mathbf{e}_{xB}$ axis such that the angle is minimum at the end of the downstroke, null when the wings are level, and

‡Data available online at www.flappingflight.com [retrieved 28 October 2008].

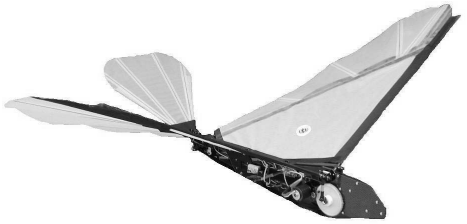

Parameter	Value	Unit
Mass	446.0	g
Overall length	0.781	m
Mean chord	0.295	m
Wing span	1.196	m
Wing area	0.329	m^2
Aspect ratio	4.360	-

Fig. 1 Ornithopter test aircraft and specifications.

a) Rotated view, showing a positive wing angle **b) Side view, showing a negative longitudinal tail deflection** **c) Back view, showing a negative lateral tail deflection**

Fig. 2 Sign conventions for the wing and tail deflection angles.

maximum at the end of the upstroke. The longitudinal tail deflection $\theta_2 \in [-50 \text{ deg}, -18 \text{ deg}]$ and lateral tail deflection $\theta_3 \in [-40 \text{ deg}, +40 \text{ deg}]$ are defined as the pitch and roll angles of the tail about the $\mathbf{e}_{yB}$ and $\mathbf{e}_{xB}$ axes, respectfully. These sign conventions are consistent with those used with fixed-wing aircraft in that negative deflections induce positive on-axis torques about the aircraft center of mass [11].

In contrast to conventional aircraft, the center of mass location for the ornithopter is not stationary and migrates along the $\mathbf{e}_{zB}$ axis 0.10 m, which is 12.8% of the overall length and 8.36% of the wingspan. A multibody model, consisting of the fuselage, the two wings, and the two parts which compose the tail mechanism, was created to model the mass distribution. Using knowledge of the wing and tail deflection angles, the center of mass location can be determined and accelerometer measurements can be corrected [11,12] using

$$\mathbf{a}^B = \mathbf{R}^{BS}\mathbf{a}^S + \frac{1}{g}[(\boldsymbol{\omega}^B)^T(\boldsymbol{\omega}^B)\mathbb{I} - (\boldsymbol{\omega}^B)(\boldsymbol{\omega}^B)^T - \mathbf{S}(\dot{\boldsymbol{\omega}}^B)]\mathbf{r}_{SB} \quad (1)$$

where g is the gravitational acceleration, $\mathbb{I}$ is the identity matrix, and $\mathbf{S}(\cdot)$ is the matrix representation of the cross-product operation. Rotational acceleration estimates are computed by smoothly differentiating the gyroscope measurements [13,14]. Measurements which are not corrected to the center of mass have additional contributions from centripetal acceleration.

III. Avionics Hardware

An avionics package [15], shown in Fig. 3, was constructed to collect sensor measurements and log data during flight. Fully assembled, the avionics package has a 0.044 m by 0.070 m footprint and a 27.9 g mass. The avionics are controlled with a reprogrammable PIC18F8722 microprocessor running at 40 MHz. During flight, data are logged to a removable memory card capable of storing over 1 GB of information. Analog measurements are passed through first-order low-pass remotely controlled filters with corner frequencies at 50 Hz to mitigate aliasing before quantization occurs. Typically corner frequencies are set to 25 times the maximum frequency of interest [11], but these values were set to the bandwidth of the IMU for consistent filtering of the data. Data are sampled with a 16-bit analog-to-digital converter at 146 Hz, which is limited by the write speed of the memory card. The addition of the avionics hardware added roughly 30 g of mass to the ornithopter, which was accounted for in the mass distribution model.

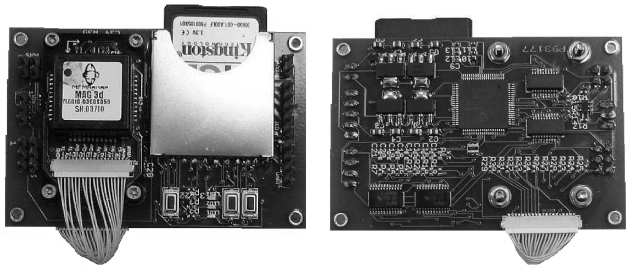

a) Obverse **b) Reverse**

Fig. 3 Avionics package.

Pilot control inputs are obtained by sampling the digital pulses between the receiver output and the actuator input. A noncontact magnetic potentiometer was used to measure the wing angle. Tail deflection angles were obtained by modifying servomotors to output the internal potentiometer signal to an amplification circuit, which could then be measured. The inertial measurement unit used is the MAG3 sensor from MemSense, which houses orthogonal triads of MEMS magnetometers, gyroscopes, and linear accelerometers. The calibration constants for the inertial measurements were determined at the time of the flight test. A calibration technique developed by Gebre-Egziabher et al. [16] was used to calibrate the magnetometer and accelerometer. Although the ornithopter was level on the ground and pointing north, magnetometer projections were recorded and used as an inertial reference vector. Gyroscopes were calibrated using a least-squares technique which enforces compatibility of the rotational kinematic equations. Ranges, resolutions, and sample variances of each sensor are given in Table 1. All measurements were of sufficient range and resolution for this study.

IV. Results

A. Flight Data

Data were collected during flight tests where the ornithopter was trimmed for straight and level mean flight. Flight tests are conducted by first powering the ornithopter and avionics equipment and then running diagnostic subroutines. The start button is pressed on the avionics package and data collection begins, followed by the launching of the ornithopter. During flight the trim settings on the radio transmitter are adjusted until the ornithopter maintains a straight and level mean flight trajectory, per visual inspection. The trim settings determined are provided in Table 2. The throttle setting is relatively high, as the current vehicle design has small margins of excess lift and thrust. The longitudinal deflection of the tail balances the weight of the ornithopter and maintains a level mean flight path trajectory. The small lateral tail deflection corrects for a slight lateral imbalance in the mass distribution of the ornithopter.

A 6.4 s segment of flight data containing 28 complete wing strokes was chosen for analysis. A confined flight space and the presence of wind gusts prohibited the use of longer segments of flight data. A representative portion of the flight data is shown in Fig. 4, where

Table 1 Hardware specifications

Measurement	Range	Resolution	Variance	Unit
Time t	——	25.6	——	μs
Throttle input u_{thr}	0–1	1.5259×10^{-3}	2.0276×10^{-6}	norm
Longitudinal input u_{lon}	$-50- -18$	0.4883×10^{-3}	2.6845×10^{-3}	deg
Lateral input u_{lat}	$-40- +40$	1.2207×10^{-3}	3.1667×10^{-3}	deg
Wing angle θ_1	$-180- +180$	5.4932×10^{-3}	24.675×10^{-3}	deg
Longitudinal deflection θ_2	$-50- -18$	0.5371×10^{-3}	36.122×10^{-3}	deg
Lateral deflection θ_3	$-40- +40$	1.3428×10^{-3}	174.18×10^{-3}	deg
Magnetic field $\mathbf{h}^S$	± 3.1667	48.319×10^{-6}	34.043×10^{-6}	norm
Rotational velocity $\boldsymbol{\omega}^S$	± 300	9.1553×10^{-3}	1.0462	deg/s
Linear acceleration $\mathbf{a}^S$	± 10	0.3052×10^{-3}	0.2507×10^{-3}	g

Table 2 Trimmed control settings for straight and level mean flight

Measurement	Value	Unit
Throttle setting u_{thr}	0.81	Normalized
Longitudinal deflection u_{lon}	-37	deg
Lateral deflection u_{lat}	-1	deg

measurements have been plotted on similar scales to emphasize the relative amplitudes. Accelerometer measurements have been corrected to the center of mass using Eq. (1). The root wing angle has a maximum amplitude of 25 deg and is approximately sinusoidal, which is expected because a simple crankshaft mechanism is used. Magnetometer signals vary only along the $\mathbf{e}_{xB}$ and $\mathbf{e}_{zB}$ axes because the motion of the ornithopter is primarily in the longitudinal plane during straight and level mean flight. The measured lateral magnetic projections are steady and small in amplitude because the ornithopter is flown in a straight path with a heading almost parallel with the vector used for the magnetic reference. The roll, pitch, and yaw rate measurements have maximum amplitudes of 265, 322, and 124 deg/s, respectfully. Although periodicity is evident, the roll and yaw rate measurements are small in amplitude and contain high frequency content. The pitch rate, however, is large in amplitude and of lower frequency content. Although an approximate result, integrating the pitch rate to obtain the pitch angle perturbation and detrending the result to remove numerical integration drift shows that the pitch angle undergoes a ± 9 deg perturbation over the course of a wing stroke. The longitudinal, lateral, and heave accelerations have maximum amplitudes of 1.9, 1.2, and 4.7 g, respectfully. High and low frequency content is visible in all three sensor channels, although it is clear that there is one dominant frequency in the longitudinal acceleration. Again an approximate calculation, gravitational acceleration can be removed from the heave acceleration measurement using the integrated pitch rate measurement. The heave acceleration can then be integrated once for the heave velocity perturbation, and twice for the altitude perturbation. This method estimates that during the wing stroke the vertical heave velocity and altitude undergo oscillations with 0.9 m/s and 0.030 m amplitudes, respectfully. The frequency rich spectra of the longitudinal acceleration prevents this calculation for estimating longitudinal velocity and position perturbations.

The measured flight data are transformed into the frequency domain to illuminate the harmonics seen in the time domain data and are shown in Fig. 5. A mean pitch angle accounts for the bias content

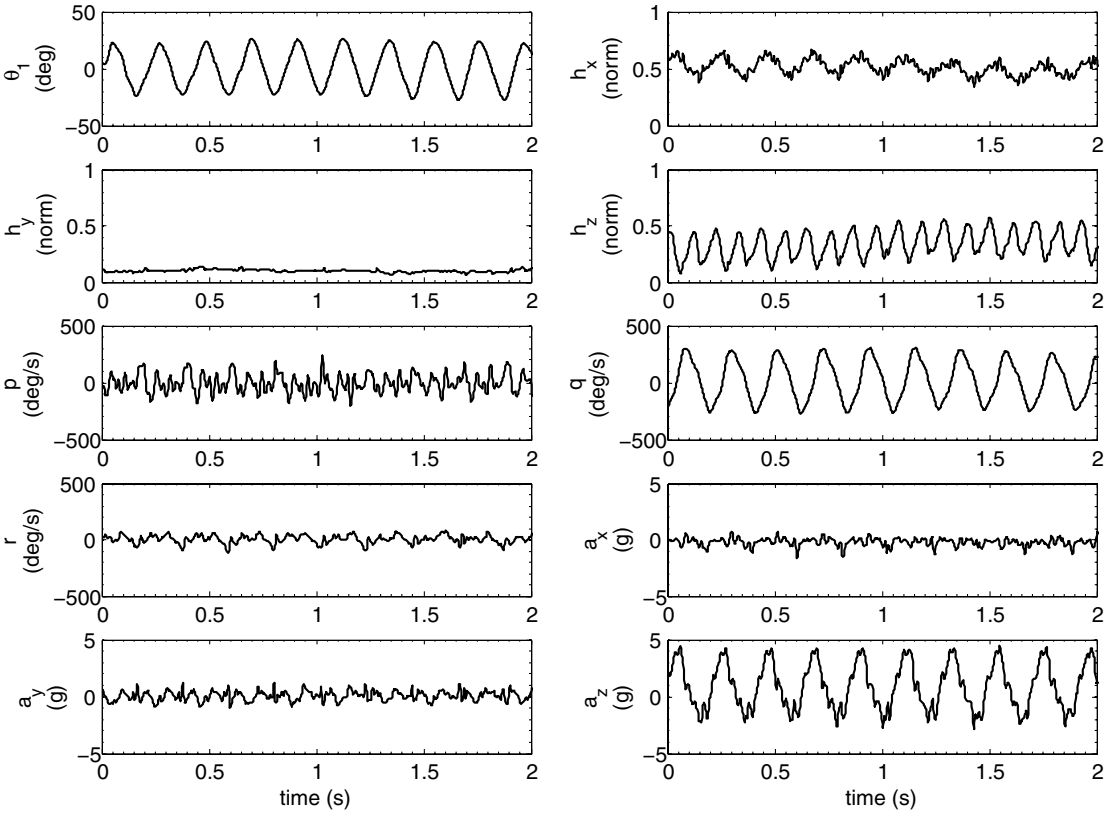

Fig. 4 Representative measurements in straight and level mean flight.

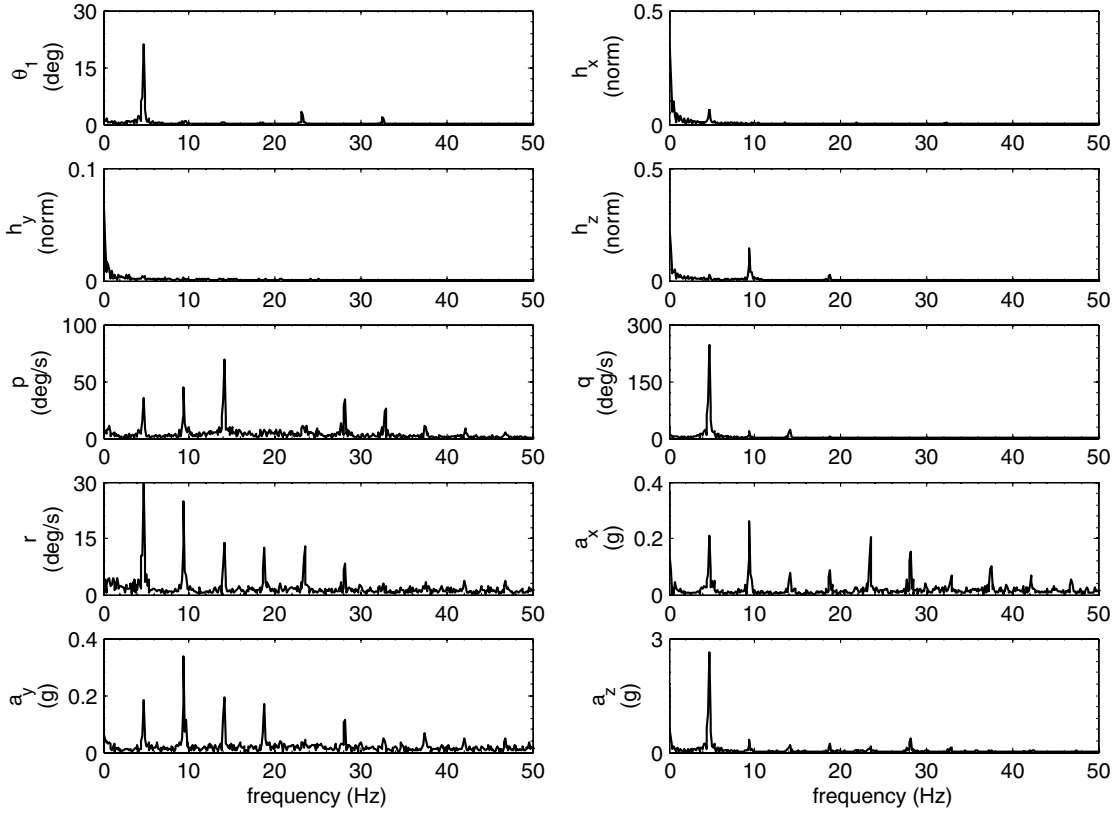

Fig. 5 Fourier coefficients of the measured flight data.

seen in the longitudinal and heave magnetic projections, whereas the bias in the lateral projection is due to a steady heading angle. The bias content seen in the longitudinal and heave accelerometers are the contributions of acceleration from gravity in the mean trimmed pitch angle orientation. The fundamental frequency seen in the spectra is the 4.69 Hz flapping frequency of the wings, which generates 1/rev lift and thrust forces registered by the longitudinal and heave accelerometers, which then generate pitching moments on the

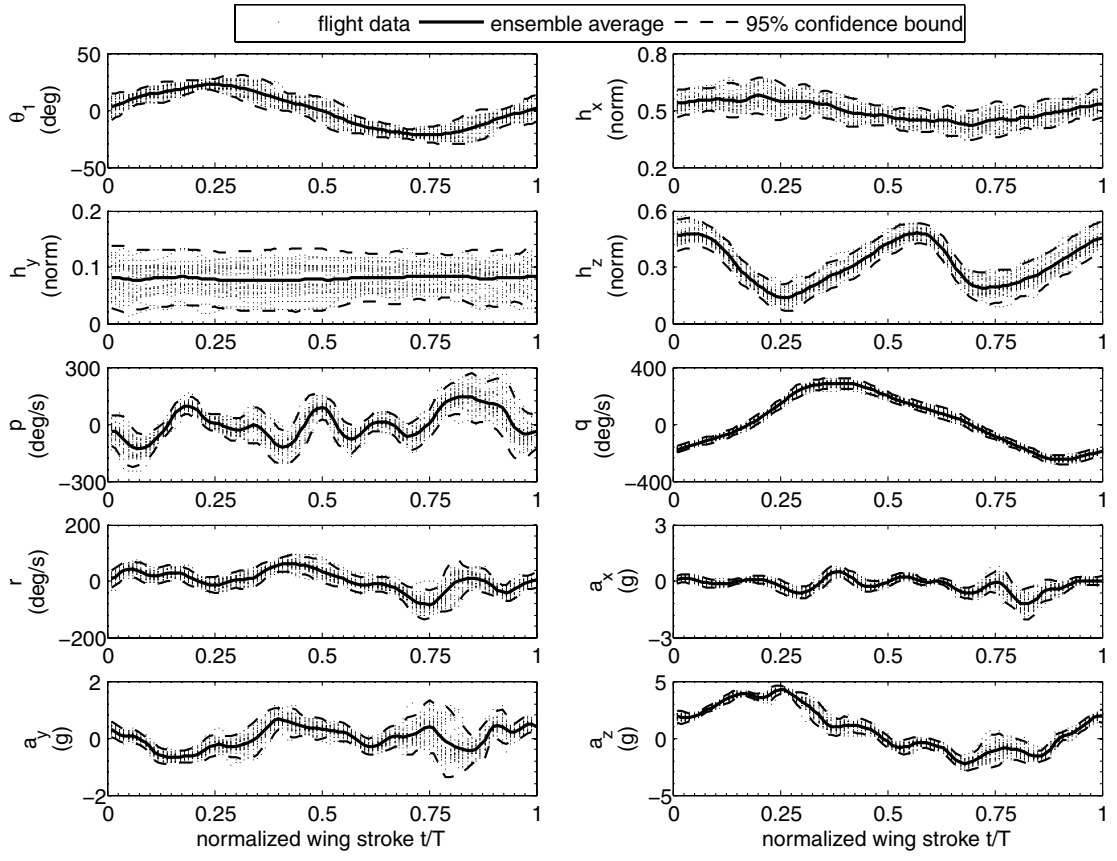

Fig. 6 Ensemble average of the measured flight data.

aircraft. Additionally the pitch angle oscillates at this frequency, which contributes gravitational acceleration to the spectral amplitudes of the accelerometers. The frequency content seen at the first harmonic in the longitudinal acceleration is due to the 2/rev thrust component. Analysis using first principles modeling [17] and computational fluid dynamics [18] is consistent with the explanation of the longitudinal and heave accelerometer measurements. The sources of the remaining amplitudes are not known exactly, but are suspected to be vibrations excited by the flapping wings. Spectral content in the roll rate, pitch rate, and lateral acceleration are expected to be caused by bending and torsion modes in the fuselage, which have been seen in high-speed images taken of the ornithopter during flight. Analysis of an experiment measuring wing shape using a visual tracking system showed that the primary wing spars undergo bending and lead–lag motions during the wing stroke [17,18]. These motions are expected to contribute to the high frequency content in the wing angle and longitudinal accelerometer measurements.

B. Representative Wing Stroke

Ensemble averaging methods enhance signal-to-noise ratios and produce representative waveforms of periodic signals [19,20]. These methods have been employed to improve measurements of electrocardiographs [21] and determine structural failures in the health monitoring of helicopter transmissions [22]. For a band-limited, deterministic signal $x(t)$ with periodicity T, a measurement model can be postulated as

$$z(t) = x(t) + v(t) \tag{2}$$

where $v(t)$ is zero-mean, wide-sense stationary sensor noise. The ensemble average and variance are then

$$\eta_z(t) = \frac{1}{N}\sum_{n=0}^{N-1} z(t + nT) \tag{3}$$

$$\sigma_z^2(t) = \frac{1}{N}\sum_{n=0}^{N-1}[z(t + nT) - \eta_z(t)]^2 \tag{4}$$

where N is the number of complete periods measured. A bound of 2 standard deviations is used to define the confidence intervals.

The flight data are periodic signals and are amenable to ensemble averaging. The wing beat frequency is used to delimit the wing stroke, which is defined to begin when the wing angle is zero and increases through the upstroke. As the wing beat frequency does not evenly divide into the sampling frequency, measurements are interpolated into 100 evenly spaced locations through the wing stroke. Measurements, ensemble averages, and confidence intervals are shown in Fig. 6. The wing angle oscillates sinusoidally with a 25 deg amplitude; becomes zero at $0.00T$, $0.50T$, and $1.00T$; reaches at maximum value during the transition from upstroke to downstroke at $0.25T$; and obtains a minimum value during the transition from downstroke to upstroke at $0.75T$. The longitudinal magnetic projection varies at the wing beat frequency about 0.50 with a 0.10 normalized amplitude, and has extrema at $0.25T$ and $0.75T$. The lateral magnetic projection is constant. The heave magnetic projection oscillates about 0.32 with a 0.15 normalized amplitude and has extrema at $0.04T$, $0.26T$, $0.57T$, and $0.73T$. The waveforms for the roll rate, yaw rate, longitudinal acceleration, and lateral acceleration have several peaks along the wing stroke. The pitch rate measurement reaches a maximum value of $+285$ deg/s at $0.40T$ and a minimum value of -250 deg/s at $0.90T$. The heave accelerometer measurement reaches a maximum value of $+4.25$ g at $0.25T$ and a minimum value of -2.22 g at $0.68T$. The cross correlation of the measurements with the wing angle is defined as

$$\mathcal{R}_{\theta_1 z} = \int_{-\infty}^{\infty} \theta_1(t + \tau)z(\tau)\,\mathrm{d}\tau \tag{5}$$

and is useful for characterizing the lag index τ between measurements with a similar waveform. The flapping motion primarily generates a lift, which induces a heave acceleration and a pitch rate. The longitudinal magnetic projection, pitch rate, and heave acceleration have strong correlations with the wing angle and lag behind by $0.30T$.

Figure 7 shows the variance of the measurements about the ensemble averages and is provided to magnify the distribution of

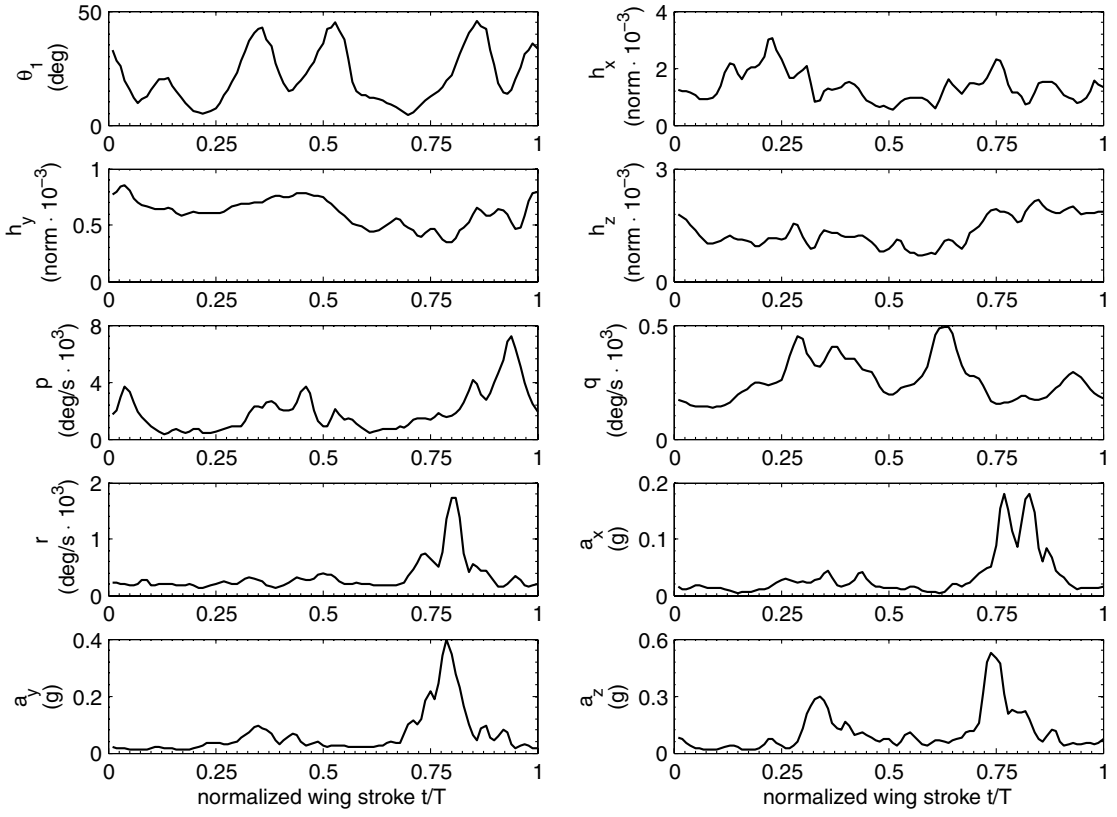

Fig. 7 Sample variance of the measured flight data about the ensemble average.

flight data about the ensemble average. The variance of the wing angle has a set of two peaks which are formed after the transitions between the upstroke and the downstroke. Magnetometer measurements have only small changes in variance over the wing stroke. The rotational velocity and linear acceleration measurements typically have large peaks in the variance after $0.75T$, which may indicate unsteady aerodynamic forcings generated at the transition between downstroke and upstroke. Although peaks are also evident in these measurements after $0.25T$ where the wing angle transitioned from upstroke to downstroke, the peaks are much smaller.

V. Conclusions

This paper presents measurements of wing angle, magnetic projection, rotational velocity, and linear acceleration, collected from a flapping-wing ornithopter in straight and level mean flight. A time domain view of the data allows a straightforward characterization of amplitudes and trends, whereas a frequency domain view of the data illuminated the amplitudes of the harmonic frequencies measured. Ensemble averaging is used to generate representative waveforms over the duration of the wing stroke with associated statistics.

The wing angle was seen to be evenly divided between the upstroke and the downstroke. This is characteristic of man-made flapping devices, but is in sharp contrast to actual birds, where the downstroke is noticeably longer than the upstroke and can be actively modulated. The frequency of the wing stroke and its harmonics were seen to be the dominant frequencies in the inertial measurements. Future vehicle designs may include mechanisms to augment the wing stroke in order to manipulate the resulting forces and moments on the ornithopter. Additionally it is interesting to note that empirical trends of birds [23] predict the flapping frequency of the ornithopter to be 2.67 Hz, which is roughly half the current rate and indicates vehicle design still has much potential.

In straight and level mean flight the ornithopter was seen to experience pitch rates of 285 deg/s and heave accelerations of 4.25 g. These are fast motions for an aircraft, especially in the most simple case of straight and level flight. These facts have important implications in the application of attitude estimation algorithms. First, simple calculations which assume small angle perturbations, for example, calculating heading from a two-axis magnetometer, cannot be used. Additionally accelerometers measured loadings several times the amount of gravity, and so low acceleration assumptions cannot be used to extract roll and pitch angles from accelerometers. Without estimates of orientation, the drift resulting from the numerical integration of the angular velocities cannot be corrected for, as in complimentary filtering techniques. Although more exotic methods may be used in some instances, it is expected that attitude estimation will have to be performed in a model-based state observer, combining numerous measurements of the vehicle dynamics.

Many of the harmonics measured by the gyroscopes and accelerometers are expected to be structural vibrations in the fuselage. These vibrations are disturbances to the measurements and degrade the quality of the measurements and any attempts to use them to estimate the vehicle attitude. It is recommended that the vehicle design be strengthened. If flight performance suffers, additional sensors can be added to measure and model the flexibility in the fuselage.

Acknowledgments

The authors would like to thank the NASA Langley Research Center, the National Institute of Aerospace, and the University of Maryland for their support in this research. Also the authors would like to thank the members of the Morpheus Laboratory for their teamwork and motivation.

References

[1] Raney, D., and Slominski, E., "Mechanization and Control Concepts for Biologically Inspired Micro Air Vehicles," *AIAA Guidance, Navigation, and Control Conference and Exhibit*, AIAA, Reston, VA, 11–14 Aug. 2004.

[2] Keennon, M., and Grasmeyer, J., "Development of the Black Widow and Microbat MAVs and a Vision of the Future of MAV Design," *International Air and Space Symposium and Exposition*, AIAA, Reston, VA, July 2003.

[3] Mueller, T., and DeLaurier, J., "An Overview of Micro Air Vehicle Aerodynamics," *Fixed and Flapping Wings Aerodynamics for Micro Air Vehicle Applications*, edited by T. Mueller, Progress In Aeronautics and Astronautics, AIAA, Reston, VA, 2001, pp. 1–10.

[4] Bohorquez, F., Samuel, P., Sirohi, J., Pines, D., Rudd, L., and Perel, R., "Design, Analysis, and Hover Performance of a Rotary Wing Micro Air Vehicle," *Journal of the American Helicopter Society*, Vol. 48, No. 2, April 2003, pp. 80–90.

[5] Shuster, M., and Oh, S., "Three-Axis Attitude Determination from Vector Observations," *Journal of Guidance and Control*, Vol. 4, No. 1, Jan.–Feb. 1981, pp. 70–77. doi:10.2514/3.19717

[6] Crassidis, J., Markley, L., and Cheng, Y., "Survery of Nonlinear Attitude Estimation Techniques," *Journal of Guidance, Control, and Dynamics*, Vol. 30, No. 1, Jan.–Feb. 2007, pp. 12–28. doi:10.2514/1.22452

[7] Rashid, T., "The Flight Dynamics of a Full-Scale Ornithopter," M.Sc. Thesis, University of Toronto, Toronto, Canada, 1995.

[8] Dietl, J., and Garcia, E., "Stability in Ornithopter Longitudinal Flight Dynamics," *Journal of Guidance, Control, and Dynamics*, Vol. 31, No. 4, July–Aug. 2008, pp. 1157–1162. doi:10.2514/1.33561

[9] Wu, J., and Popović, Z., "Realistic Modeling of Bird Flight Animations," *ACM Transactions on Graphics*, Vol. 22, No. 3, July 2003, pp. 888–895. doi:10.1145/882262.882360

[10] McRuer, D., Ashkenas, I., and Graham, D., *Aircraft Dynamics and Automatic Control*, Princeton Univ. Press, Princeton, NJ, 1973.

[11] Klein, V., and Morelli, E., *Aircraft System Idenfication: Theory and Practice*, AIAA Education Series, AIAA, Reston, VA, 2006.

[12] Gainer, T., and Hoffman, S., "Summary of Transformation Equations and Equations of Motion Used in Free-Flight and Wind-Tunnel Data Reduction and Analysis," NASA TR SP-3070, Langley Research Center, 1972.

[13] Morelli, E., "Practical Aspects of the Equation-Error Method for Aircraft Parameter Estimation," AIAA Paper 2006-6144, 2006.

[14] Morelli, E., "System Identification Programs for Aircraft (SIDPAC)," AIAA Paper 2002-4704, 2002.

[15] Grauer, J., and Hubbard, J., "Development of a Sensor Suite for a Flapping-Wing UAV Platform," AIAA Paper 2008-0224, 2008.

[16] Gebre-Egziabher, D., Elkaim, G., Powell, J. D., and Parkinson, B. W., "Calibration of Strapdown Magnetometers in Magnetic Field Domain," *Journal of Aerospace Engineering*, Vol. 19, No. 2, April 2006, pp. 87–102. doi:10.1061/(ASCE)0893-1321(2006)19:2(87)

[17] Harmon, R., Grauer, J., Hubbard, J., and Humbert, S., "Experimental Determination of Ornithopter Membrane Wing Shapes Used for Simple Aerodynamic Modeling," AIAA Paper 2008-6237, Aug. 2008.

[18] Sitaraman, J., Roget, B., Harmon, R., Grauer, J., Conroy, J., Hubbard, J., and Humbert, S., "A Computational Study of Flexible Wing Ornithopter Flight," AIAA Paper 2008-6397, Aug. 2008.

[19] Braun, S., "The Extraction of Periodic Waveforms by Time Domain Averaging," *Acustica*, Vol. 32, No. 2, 1975, pp. 69–77.

[20] Hochmann, D., and Sadok, M., "Theory of Synchronous Averaging," *IEEE Aerospace Conference Proceedings*, IEEE, Piscataway, NJ, 2004, pp. 3636–3653.

[21] Lander, P., and Berbari, E., "Use of Time-Frequency Representations to Enhance the Signal-to-Noise Ratio of the Signal-Averaged ECG," *Computers in Cardiology*, IEEE, Piscataway, NJ, Oct. 1992, pp. 451–454.

[22] Samuel, P., "Helicopter Transmission Diagnostics Using Constrained Adaptive Lifting," Ph.D. Thesis, University of Maryland, College Park, MD, 2003.

[23] Pennycuick, C., "Predicting Wingbeat Frequency and Wavelength of Birds," *Journal of Experimental Biology*, Vol. 150, No. 1, 1990, pp. 171–185.